JACS
JOURNAL OF THE AMERICAN CHEMICAL SOCIETY
Article
pubs.acs.org/JACS

Experimental and Computational Assessment of Reactivity and Mechanism in C(sp^3)−N Bond-Forming Reductive Elimination from Palladium(IV)

Ian M. Pendleton,[‡] Mónica H. Pérez-Temprano,[‡] Melanie S. Sanford,* and Paul M. Zimmerman*

Department of Chemistry, University of Michigan, Ann Arbor, Michigan 48109, United States

Supporting Information

ABSTRACT: This report describes a combined experimental and computational investigation of the mechanism of C(sp^3)−N bond-forming reductive elimination from sulfonamide-ligated Pd^{IV} complexes. After an initial experimental assessment of reactivity, we used ZStruct, a computational combinatorial reaction finding method, to analyze a large number of multistep mechanisms for this process. This study reveals two facile isomerization pathways connecting the experimentally observed Pd^{IV} isomers, along with two competing S$_N$2 pathways for C(sp^3)−N coupling. One of these pathways involves an unanticipated oxygen−nitrogen exchange of the sulfonamide ligand prior to an inner-sphere S$_N$2-type reductive elimination. The calculated $\Delta G^{\ddagger}$ values for isomerization and reductive elimination with a series of sulfonamide derivatives are in good agreement with experimental data. Furthermore, the simulations predict relative reaction rates with different sulfonamides, which is successful only after considering competition between the proposed operating mechanisms. Overall, this work shows that the combination of experimental studies and new computational tools can provide fundamental mechanistic insights into complex organometallic reaction pathways.

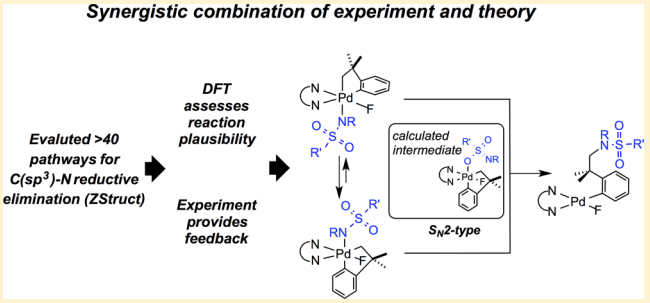

INTRODUCTION

Over the past decade, Pd-catalyzed C(sp^3)−N bond forming reactions (involving both C−H amination and oxidative amination of alkenes) have emerged as valuable methods in organic synthesis.[1,2] Although high-valent palladium complexes have been proposed as intermediates in these transformations, a detailed mechanistic understanding of the key C(sp^3)−N bond-forming step has remained largely elusive.[3,4] Recently, we isolated a Pd^{IV} model complex, **1**$_{Ts}$, that undergoes selective C(sp^3)−N coupling (Scheme 1).[5] This work was the first example of C(sp^3)−N bond-forming reductive elimination from a well-defined Pd^{IV} complex.[6]

Scheme 1. C(sp^3)−N Bond-Forming Reductive Elimination from 1$_{Ts}$

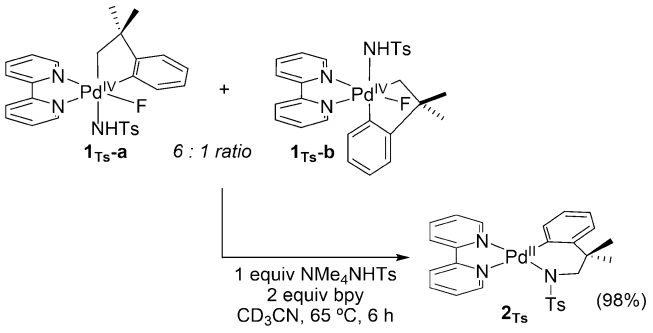

A detailed mechanistic understanding of this C(sp^3)−N coupling process would provide valuable information about relative rates, ligand design, and stereochemistry that could ultimately inform new catalyst design and optimization. However, experimental mechanistic studies of reductive elimination from **1**$_{Ts}$ are hampered by the complexity of this system. For example, two different isomers of this octahedral Pd^{IV} complex (**1**$_{Ts}$**-a** and **1**$_{Ts}$**-b**) are detectable, and others could be kinetically accessible under the reaction conditions. Furthermore, multiple kinetically indistinguishable reductive elimination pathways are possible from each of these isomers (vide infra).

The complexity of these competing reductive elimination pathways motivated us to pursue computational studies to gain a greater understanding of this transformation. We reasoned that this system would serve as an attractive test case for the ZStruct program, a new reaction-finding tool developed in the Zimmerman lab.[7] ZStruct enables a combinatorial exploration of reaction pathways originating from an initial species (Figure 1) and uses quantum chemistry to provide accurate analysis of the thermodynamic and kinetic factors that govern each path. The entire set of ZStruct-discovered reaction pathways are automatically characterized at the full level of detail and accuracy available to modern quantum chemical simulations of reaction mechanism. In comparison to a traditional DFT

Received: March 17, 2016
Published: April 18, 2016

DOI: 10.1021/jacs.6b02714
J. Am. Chem. Soc. 2016, 138, 6049−6060

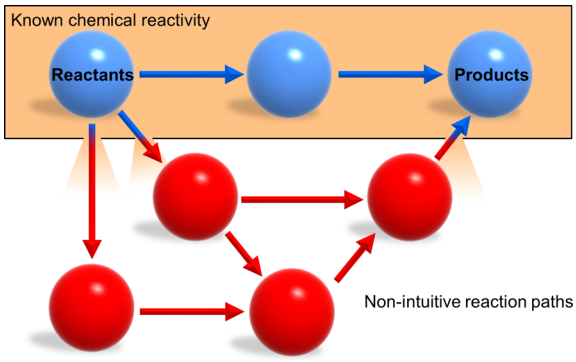

Figure 1. ZStruct mediated mechanism discovery incorporates known and nonintuitive chemical pathways.

investigation, this method significantly expands the scope of reactivity and can reveal previously unknown mechanistic pathways. Importantly, the advantages of this method must be balanced by its high computational cost relative to traditional DFT.[8] However, with the rapidly expanding availability of computational power, ZStruct and other modern reaction network discovery tools[9] are expected to become more and more economical for mechanistic investigations in years to come.

We report herein that combining experimental studies with ZStruct allowed us to unravel competing pathways for carbon–nitrogen bond-forming reductive elimination from complex $\mathbf{1}_{Ts}$ and derivatives thereof. During these studies, ZStruct unveiled an unanticipated, alternative pathway for C(sp^3)–N coupling at Pd^{IV} alkyl sulfonamide complexes. This pathway, shown in Scheme 2, is an inner-sphere, concerted reductive elimination

Scheme 2. New Pathway for C(sp^3)–N Reductive Elimination of Sulfonamide Substrates Discovered by ZStruct

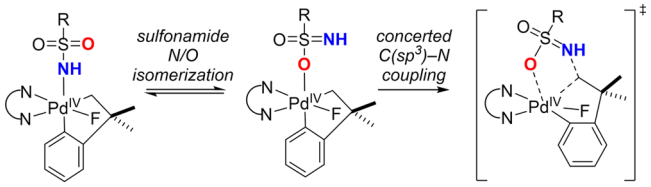

via a 5-membered transition state that does not require predissociation of the sulfonamide. Prior literature reports have shown that C(sp^3)–C(sp^2)[10] and C(sp^2)–X reductive elimination processes from high-valent group 10 complexes occur through concerted inner-sphere mechanisms, while C(sp^3)–heteroatom[11–14] couplings generally favor outer-sphere S_N2-type mechanisms. To our knowledge, concerted inner-sphere paths have not been previously implicated for C(sp^3)–N coupling.[15,16] However, as detailed below, in our system, it is necessary to invoke competing inner and outer-sphere C(sp^3)–N reductive elimination mechanisms to fully explain the experimental data. Overall, this work leverages a synergistic combination of experimental studies and ZStruct to obtain a detailed mechanistic picture of C(sp^3)–N bond-forming reductive elimination from $\mathbf{1}_{Ts}$ and its analogues.

RESULTS AND DISCUSSION

1. Possible Mechanisms for C(sp^3)–N Reductive Elimination from Pd^{IV} Complexes. We initially considered 4 mechanisms for reductive elimination from Pd^{IV} complexes of general structure **1**. All of these mechanisms have significant precedent in the literature for other carbon-heteroatom bond-forming reductive elimination processes.[17–20]

The first possibility (pathway **Ia**/**b**) involves direct nucleophilic attack by exogeneous RNH^- on the six-coordinate Pd^{IV} starting complex. As shown in Scheme 3, this encompasses two distinct processes, as it could occur from either isomer **1a** or isomer **1b**. The rate expression for each is expected to be similar and is shown in Scheme 3.

Scheme 3. Pathway I: Direct Nucleophilic Attack

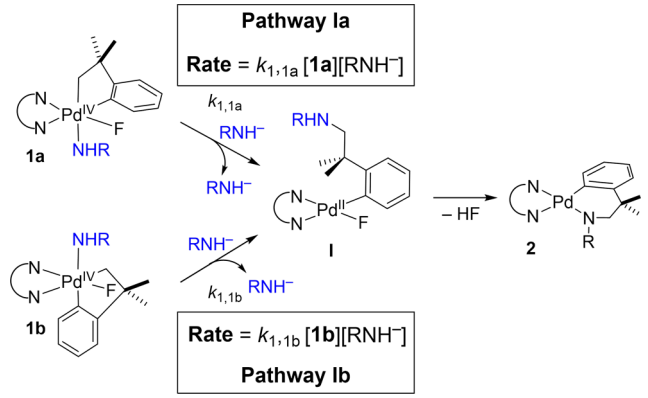

Pathway **II** involves the dissociation of one arm of the bipyridine ligand to generate a neutral 5-coordinate intermediate, followed by concerted C–N reductive elimination via a traditional 3-membered transition state. This pathway is only possible for isomer **1b**, since the sulfonamide and σ-alkyl ligands are *trans* to one another in **1a**. Because Pd^{IV} complex **1b** is unsymmetrical, this pathway could involve two different neutral pentacoordinate Pd^{IV} intermediates. In these two-step mechanisms, either the ligand dissociation or C–N coupling could be the rate-determining step. The rate expression for each possibility is shown in Scheme 4.

Pathway **III** proceeds via concerted C(sp^3)–N bond-forming reductive elimination (via a traditional 3-membered transition state) from the octahedral palladium center of **1b**. This pathway is not possible for **1a**, since the sulfonamide and σ-alkyl ligands

Scheme 4. Pathway II: Bipyridine Ligand Dissociation

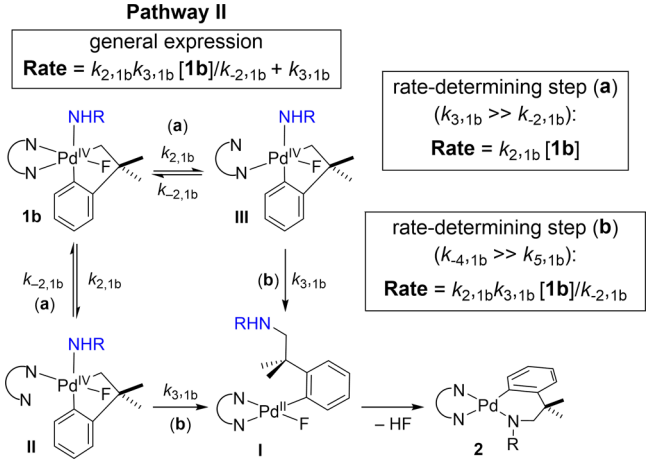

DOI: 10.1021/jacs.6b02714
J. Am. Chem. Soc. 2016, 138, 6049–6060

are *trans* to one another in this isomer. This mechanism and the corresponding rate expression are shown in Scheme 5.

Scheme 5. Pathway III: Concerted Reductive Elimination

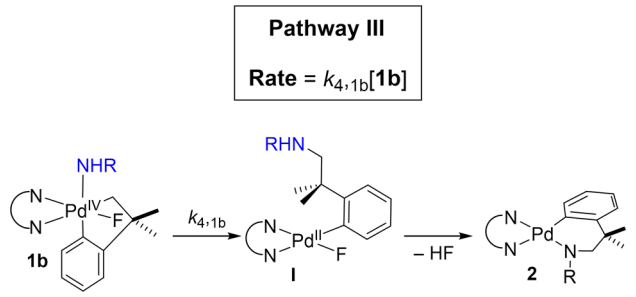

Finally, pathway **IVa/b** involves two-steps: pre-equilibrium dissociation of RNH^- to afford a 5-coordinate cationic intermediate followed by S_N2-type attack of RNH^- on the Pd-σ-alkyl intermediate. As in the previous two-step mechanisms, either the ligand dissociation or the C–N coupling could be the rate-determining step. The rate expressions for each of these possibilities are shown in Scheme 6.

Scheme 6. Pathway IV: S_N2 Pathway

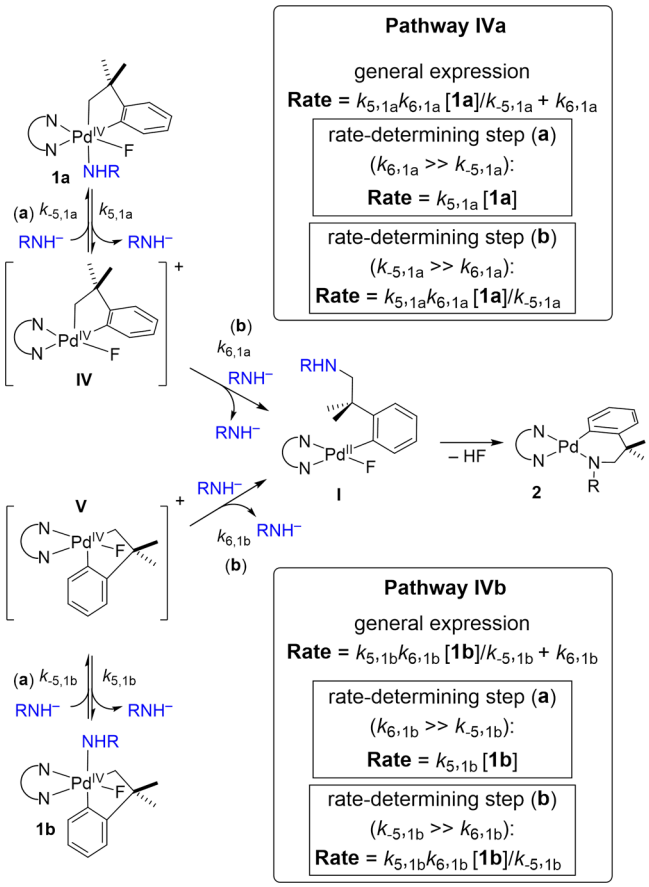

1.1. Previous Studies of $\mathbf{1}_{Ts}$. Our initial communication provided preliminary mechanistic insights into C(sp^3)–N bond-forming reductive elimination from $\mathbf{1}_{Ts}$.[5] These studies showed that the reaction exhibits a first-order dependence on [$\mathbf{1}_{Ts}$] and zero-order dependence on [NMe_4NHTs]. These data unambiguously rule out pathway **I**, but do not allow us to differentiate between pathways **II**–**IV**. We also observed rapid exchange between free and Pd-bound $TsNH^-$ at temperatures significantly lower than those required for C(sp^3)–N coupling.[21] This indicates that the sulfonamide dissociation step of pathway **IV** is fast under our reaction conditions.

2. Experimental Studies of C(sp^3)–N Coupling.

2.1. Initial Screen of Sulfonamide Nucleophiles. Using the results with $\mathbf{1}_{Ts}$ as starting point, we first studied C(sp^3)–N bond-forming reductive elimination as a function of nucleophile with a series of sulfonamides.[22] The sulfonamides $CF_3SO_2NH^-$, $CF_2HSO_2NH^-$, and $CH_3SO_2NH^-$ were selected to represent a range of electronic properties (i.e., pK_a values). A fourth sulfonamide, $TsMeN^-$ was selected to alter the steric properties and hydrogen bond donor ability of the nucleophile, while maintaining similar pK_a to $TsNH^-$.

The concentrations of the Pd^{IV} starting materials and of the reductive elimination products were monitored via ^1H NMR spectroscopy. The rate constant (k_{C-N}) with each sulfonamide was determined by fitting the concentration versus time data to the kinetic model proposed in Figure 2 (rate = k_{C-N}[$\mathbf{1}_R$]).

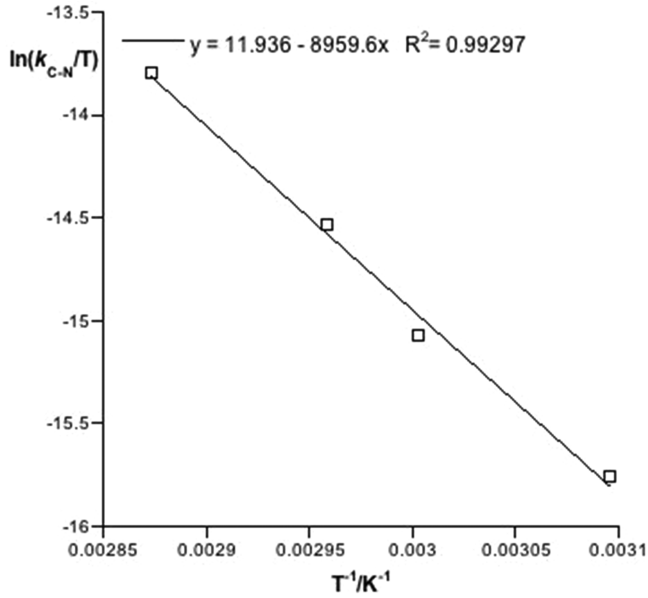

Figure 2. Eyring plot for determination of $\Delta H^{\ddagger}$ and $\Delta S^{\ddagger}$ for the C(sp^3)–N reductive elimination from $\mathbf{1}_{Ms}$.

During the fitting of the kinetic data, the concentrations of $\mathbf{1}_R$**-a** and $\mathbf{1}_R$**-b** were added together and treated as a single Pd^{IV} complex. As summarized in Table 1, changing the steric and electronic properties of the sulfonamide had a significant impact on k_{C-N}. The fastest reaction was observed with the most electron deficient sulfonamide $CF_3SO_2NH^-$ (k_{C-N} = 6.59 × 10^{-4} s^{-1}; entry 1). The slowest reactions were observed with $CH_3SO_2NH^-$ and $TsNH^-$, which react approximately 5-fold slower than $CF_3SO_2NH^-$ (1.65 × 10^{-4} and 1.43 × 10^{-4} s^{-1}, respectively). Previous studies of related C(sp^3)–O coupling reactions from Pt^{IV} complexes showed that electron deficient benzoate derivatives react significantly faster than electron rich derivatives (Hammett ρ value = +1.44 for this system). On the basis of this prior work, we anticipated that we might observe faster rates with more electron deficient sulfonamides (i.e., sulfonamides with lower pK_a values).[19e] While this general trend is observed in Table 1, entries 1–4, the disubstituted sulfonamide ($TsMeN^-$, entry 5) is a clear outlier. This latter

DOI: 10.1021/jacs.6b02714
J. Am. Chem. Soc. 2016, 138, 6049–6060

Table 1. Reductive Elimination Reaction Rate Constant for C(sp^3)−N Coupling Using Different Sulfonamides

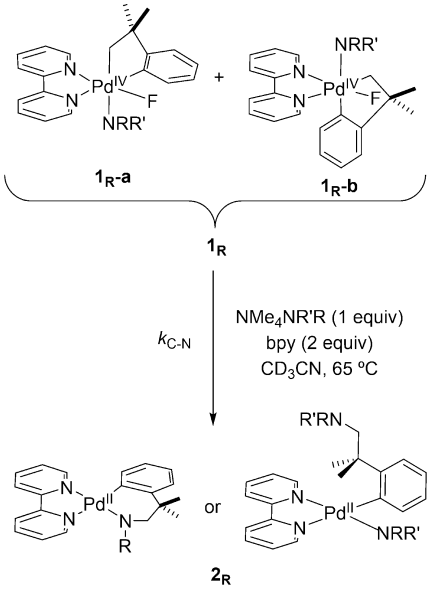

entry	R	R′	pK_a[a]	$k_{C-N,65°C}$ (10^{-4} s^{-1})
1	CF_3SO_2 (Tf)	H	6.37	6.59
2	CF_2HSO_2	H	7.46	3.87
3	CH_3SO_2 (Ms)	H	10.87	1.65
4	p-tolylSO_2 (Ts)	H	10.26	1.43
5	p-tolylSO_2 (Ts)	Me	11.67	4.75

[a] pK_a values from the literature database of ACD/Laboratories Software version 11.02. All of the reported pK_a values are for the neutral sulfonamide (R_2NH).

sulfonamide has the highest pK_a value, but shows an unexpectedly fast rate.

2.2. C(sp^3)−N Reductive Elimination from $\mathbf{1}_{Tf}$, $\mathbf{1}_{Ms}$, *and* $\mathbf{1}_{TsNMe}$. We next pursued more detailed investigations of the complexes containing $TfNH^-$, $MsNH^-$, and $TsMeN^-$. These were selected because: (1) they encompass the largest range of steric and electronic properties of the sulfonamides examined; (2) they are also among the fastest and slowest reacting; (3) they include the key outlier with respect to the initially expected pK_a trend ($TsMeN^-$); and (4) computational results suggest that a change in mechanism occurs between these nucleophiles (vide infra).

We established the kinetic orders of the C−N reductive elimination process in [Pd^{IV}] and [sulfonamide] for $\mathbf{1}_{Tf}$, $\mathbf{1}_{Ms}$, and $\mathbf{1}_{TsNMe}$. In all cases, these reactions exhibited a first-order dependence on [Pd^{IV}][23] and a zero-order dependence on [sulfonamide].[24] As discussed above for $\mathbf{1}_{Ts}$, this data allows us to definitively rule out a direct S_N2 mechanism (pathway **I** in Scheme 3), since this would exhibit a first-order dependence on sulfonamide.[25]

We next explored the feasibility of pathway **II**, which involves pre-equilibrium dechelation of the bipyridine ligand prior to C−N bond-formation. If dissociation of one of the nitrogen arms of the ligand were occurring, we would expect to see a large rate difference as a function of the rigidity of the bidentate ligand. To test this possibility, we synthesized complex $\mathbf{1'}_{Tf}$, in which the bipyridine is replaced with electronically similar but more rigid phenanthroline. As shown in Scheme 7, the rate of reductive elimination from these two complexes under our optimal conditions was essentially identical ($k_{2,bpy}$ = 6.59 × 10^{-4} s^{-1} and $k_{2,phen}$ = 6.88 × 10^{-4} s^{-1}). This experiment provides preliminary evidence against the dechelation mechanism.[26] Notably, the computational studies also strongly indicate against this mechanism (vide infra).

Scheme 7. Ligand Effects on the Rate of C(sp^3)−N Reductive Elimination

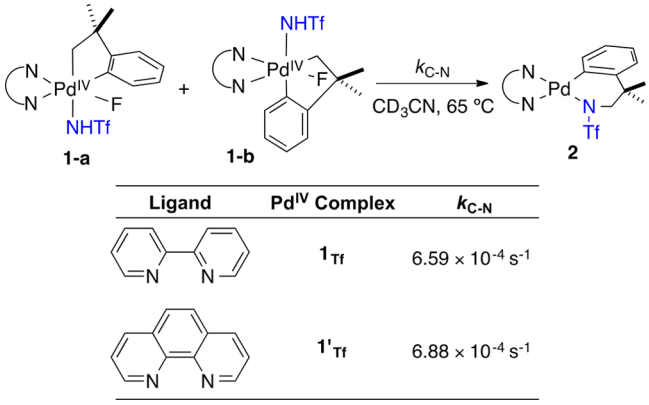

Eyring plots for C(sp^3)−N bond-forming reductive elimination from $\mathbf{1}_{Tf}$, $\mathbf{1}_{Ms}$, and $\mathbf{1}_{TsNMe}$ were obtained by monitoring the reaction rate over the temperature range of 50−75 °C. A representative plot is shown in Figure 2, and the activation parameters obtained from this analysis are provided in Table 2.

Table 2. Activation Parameters for the C(sp^3)−N Bond Forming Reaction

	$TfNH^-$	$MsNH^-$	$TsMeN^-$
$\Delta H^{\ddagger}$[a]	23.2	17.8	23.8
$\Delta S^{\ddagger}$[b]	−4.9	−23.5	−3.4
$\Delta G^{\ddagger}_{65°C}$[a]	24.8	25.7	25.0

[a] kcal·mol^{-1}. [b] cal/(mol·K).

The most noteworthy aspect of this data is the large differences in the entropy of activation between $\mathbf{1}_{Ms}$ and $\mathbf{1}_{Tf}$/$\mathbf{1}_{TsNMe}$. Specifically, the $\Delta S^{\ddagger}$ values for $\mathbf{1}_{Tf}$ and $\mathbf{1}_{TsNMe}$ are comparable to one another (−4.9 and −3.4 cal·K^{-1}·mol^{-1}, respectively) and are approximately 20 eu more positive than that for the reductive elimination from $\mathbf{1}_{Ms}$. This preliminarily suggests that different reductive elimination pathways might be operating upon variation of the sulfonamide (a proposal that is supported by computation, vide infra).

2.3. Lability of the Sulfonamide Ligand in $\mathbf{1}_{Tf}$, $\mathbf{1}_{Ms}$, *and* $\mathbf{1}_{TsNMe}$. We next examined the lability of the sulfonamide ligand in these complexes. The treatment of $\mathbf{1}_{Ms}$-**a**/$\mathbf{1}_{Ms}$-**b** with 1.2 equiv of NMe_4NHTs at room temperature resulted in fast sulfonamide exchange to form an equilibrium mixture of $\mathbf{1}_{Ms}$ and $\mathbf{1}_{Ts}$ (see Supporting Information for full details). Similar fast exchange was observed upon treatment of $\mathbf{1}_{TsNMe}$-**a**/$\mathbf{1}_{TsNMe}$-**b** with 1.2 equiv of NMe_4NHTs at room temperature. For a solution of $\mathbf{1}_{Tf}$-**a** and 3.0 equiv of NMe_4TfNH, EXSY NMR studies at 20 °C show fast exchange between free and bound $TfNH^-$. Overall, these results are similar to those obtained with $\mathbf{1}_{Ts}$, and they demonstrate that (1) sulfonamide dissociation pathways (e.g., pathway **IV**) are kinetically feasible and (2) sulfonamide dissociation is not the rate-limiting step of the C−N coupling process.

2.4. ***1-a/1-b*** *Isomerization Process.* We hypothesized that the differences in reductive elimination rates/mechanism between $\mathbf{1}_{Tf}$, $\mathbf{1}_{Ms}$, and $\mathbf{1}_{TsNMe}$ might be related to the

DOI: 10.1021/jacs.6b02714
J. Am. Chem. Soc. 2016, 138, 6049−6060

accessibility and/or reactivity of different Pd^{IV} isomers. As such, we conducted a detailed study of the isomerization process. Under our reaction conditions, all of these complexes exist as a mixture of two isomers: $\mathbf{1_R}$-**a** and $\mathbf{1_R}$-**b**.[5] However, isomer $\mathbf{1_R}$-**a** can be formed in quantitative yield via the room temperature reaction of complex **3** with NMe_4NR in CD_3CN, and it then undergoes slow isomerization to form an equilibrium mixture of $\mathbf{1_R}$-**a**/$\mathbf{1_R}$-**b** at room temperature (Scheme 8).[27] This isomerization is significantly faster than reductive elimination, and none of the C−N coupled product is detected over the time frame of isomer equilibration.

Scheme 8. $\mathbf{1_R}$-a/$\mathbf{1_R}$-b Isomerization

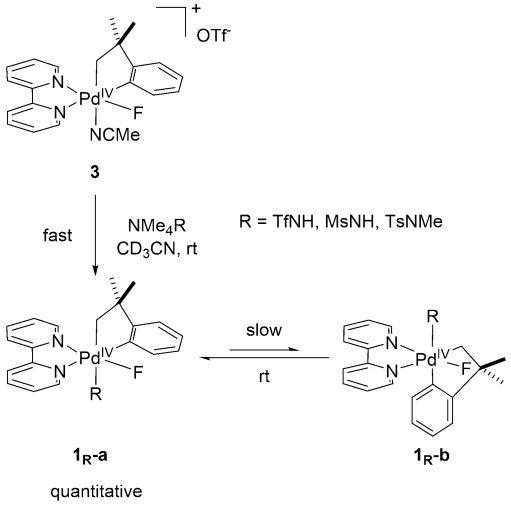

We obtained the rate and equilibrium constant for the isomerization of each complex over a range of temperatures using NMR spectroscopic analysis. Figure 3 shows the data for $\mathbf{1_{Ms}}$ as a representative example. The data were fit to the kinetic model shown in Figure 3,[28] by nonlinear least-squares (NLLS) regression.[29] The thermodynamic and activation parameters for these equilibrium processes were determined using the van't Hoff and Eyring equations, respectively. As summarized in Table 3, both the rate and equilibrium constant for isomerization vary as a function of sulfonamide. However, neither of these values correlates with the observed rate of C(sp^3)−N coupling.

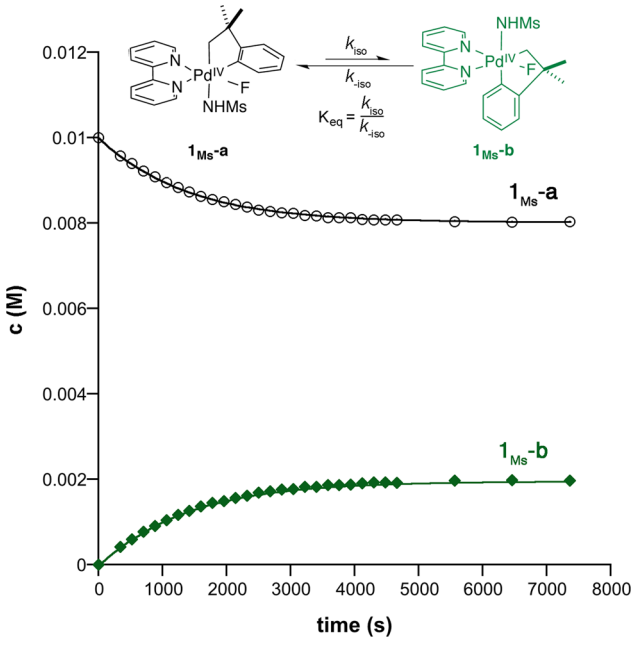

Figure 3. $\mathbf{1_{Ms}}$-a/$\mathbf{1_{Ms}}$-b isomerization process at 45 °C. Solid lines are the best fit using GEPASI.

Table 3. Thermodynamic and Activation Parameters for the Isomerization Process Using Different Sulfonamide Substrates

	$TfNH^-$	$MsNH^-$	$TsMeN^-$
ΔH^{0a}	1.08	0.21	0.06
ΔS^{0b}	−0.45	−2.16	−1.17
$\Delta G^0_{65°C}{}^a$	1.23	0.94	0.46
$K_{eq,65\ °C}$	0.16	0.24	0.51
$\Delta H^{‡a}$	18.5	19.4	21.3
$\Delta S^{‡b}$	−6.6	−14.8	−6.1
$\Delta G^‡_{65°C}{}^a$	20.7	24.4	23.4

^{a}kcal·mol^{-1}. ^{b}cal/(mol·K).

2.5. Summary and Conclusions from Experimental Studies. Overall, the experimental mechanistic studies provide several mechanistic insights into this C(sp^3)−N reductive elimination process. First, sulfonamide structure has a significant influence on the rate of reductive elimination. Second, there is not a clear trend with respect to electronic effect (pK_a) of the sulfonamide and the rate of C(sp^3)−N coupling (with sterically larger $TsNMe^-$ being the key outlier). Third, reductive elimination is first order in [Pd] and zero order in sulfonamide for all of the systems examined. Fourth, two Pd^{IV} isomers, connected by a facile isomerization step, are observed in the reaction mixture during the course of the reaction. Fifth, both isomerization and sulfonamide exchange are faster than reductive elimination.

Although the experimental studies do not provide a satisfying explanation for all these data, they allow us to rule out a direct S_N2 mechanism (pathway **I**). Furthermore, the observation of similar rates with bpy versus phen ligands suggests against the bipyridine dechelation mechanism (pathway **II**). However, these studies do not provide data to distinguish between pathways **III** and **IV**. In addition, other undetectable isomers might also be accessible (for example, **1c**, **1d**, and **1e** in Figure 4) and could potentially be involved in C(sp^3)−N coupling via related mechanisms. In combination with the possibility of at least two pathways and five different Pd^{IV} isomers, there are a minimum of 14 kinetically indistinguishable mechanisms that could be operating in this system. In addition, many of these pathways could have similar barriers (and thus be operating simultaneously), further complicating experimental mechanistic analysis. As such, we turned to ZStruct to obtain a more

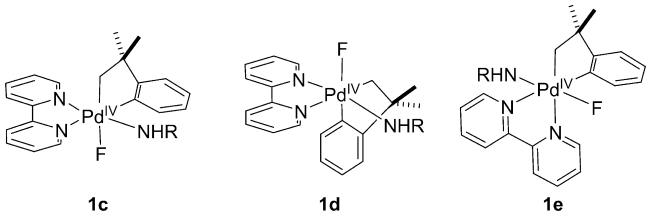

Figure 4. Possible unobserved Pd^{IV} isomers.

DOI: 10.1021/jacs.6b02714
J. Am. Chem. Soc. 2016, 138, 6049−6060

detailed mechanistic understanding of this reductive elimination reaction.

3. Identification of Isomerization Mechanism Using Computational Combinatorial Reaction Finding. *3.1. Introduction to ZStruct.* On the basis of the complexity of this system, we viewed it as an ideal test case for the computational mechanism discovery program, ZStruct.[7a,b] ZStruct is a reaction exploration tool designed to interrogate complex chemical transformations using only minimal user input. The method is able to (1) generate a large number of chemically reasonable reaction intermediates in a multistep mechanism through combinations of bond "break" and "form" operations; (2) evaluate relevant thermodynamic and kinetic parameters using DFT; and (3) utilize state-of-the-art reaction path finding methods to efficiently locate minimum energy paths and transition states.[7c−e] ZStruct differentiates axial and equatorial bonding positions of octahedral transition metal complexes and interrogates pseudorotation and axial/equatorial ligand isomerizations as well as bond-changing events. As such, it enables a full search of potentially reactive Pd^{IV} species. In comparison to a traditional DFT investigation, this method proposes and evaluates a combinatorial set of reactions in silico without substantial user intervention. This process does not require input of a predetermined set of hypothetical reaction steps, so the mechanistic pathways that are evaluated by ZStruct can be completely unexpected. ZStruct was initially developed and tested for reactions of main group compounds,[7] and the current work represents the first application to transition metal complexes.[30] A summary of these steps is shown in Scheme 9, and a full description of the method is given in the Supporting Information.

Scheme 9. Overview of the ZStruct Combinatorial Reaction Finding Tool

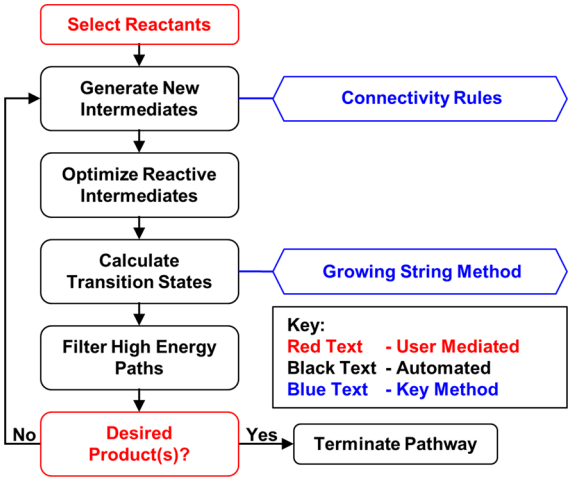

3.2. Computational Details. $\mathbf{1_{Ms}}$**-a**/$\mathbf{1_{Ms}}$**-b** were selected as chemically relevant and computationally tractable starting complexes for the ZStruct analysis. Application of ZStruct to $\mathbf{1_{Ms}}$**-a/b** generated 9482 chemical structures and 794 individual elementary steps, as well as all 794 associated transition states. During the initial assessment of reaction paths, we used the B3LYP density functional[31] in a spin restricted formalism with the LANL2DZ[32] basis set.[33] The cost of the search was approximately 80 000 computing hours, which corresponds to less than 1 week of computational time on 1000 CPUs. To narrow these pathways down to the most plausible reaction mechanisms, screening and higher-level evaluations were performed, as shown in Figure 5.

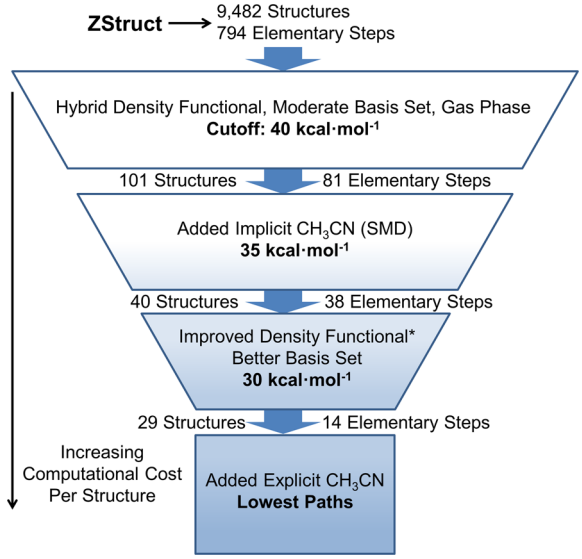

Figure 5. Screening and activation energy cutoffs ($\Delta G^{\ddagger}$) used for finding the lowest energy pathways from $\mathbf{1_{Ms}}$. *Improved density functional incorporating long-range and dispersion corrections.

The energy cutoffs were selected based on the experimentally measured barriers for isomerization and reductive elimination from $\mathbf{1_{Ms}}$**-a**. The experimental barriers, which are all less than 28 kcal·mol^{-1}, suggested that barriers more than a few kcal·mol^{-1} higher would be uncompetitive. Taking into account corrections from solvent,[34] we set the first screening cutoff at 40 kcal·mol^{-1}. After removing pathways with activation energies of ≥40 kcal·mol^{-1}, 81 elementary steps (∼10% of the total generated) remained for further analysis (first filter, Figure 5). For these elementary steps, the energies were evaluated at an implicit solvent corrected level of theory [SMD][35,36] and were subjected to a stricter energy filter of 35 kcal·mol^{-1}. This second filter reduced the key reactions to include 38 elementary steps.

The lowest energy pathways for isomerization and C(sp^3)−N reductive elimination were then analyzed using the dispersion and long-range corrected ωB97X-D density functional[37] with 6-311++G** basis set for hydrogen through sulfur and LANL2TZ(f) for Pd to provide accurate energetics.[38] For the 14 lowest barrier elementary steps (third filter), the geometries were reoptimized after adding a single explicit acetonitrile as a reagent to account for solvent binding to the palladium center (fourth filter).[39] For a more detailed description of the ZStruct method, selection of level of theory, as well as the development and application of energy cutoffs, see the Supporting Information.

3.3. Overview of ZStruct Results. As summarized in Figure 6, the ZStruct studies predicted two different, energetically viable pathways for isomerization between $\mathbf{1_{Ms}}$**-a** and $\mathbf{1_{Ms}}$**-b** as well as for C(sp^3)−N bond-forming reductive elimination. A first low energy mechanism involves the proposed sulfonamide dissociation/S_N2 pathway involving intermediate $\mathbf{4_{Ms}}$ (pathway **IV** in Figure 6). However, ZStruct also identified previously unanticipated pathways for both isomerization and C(sp^3)−N coupling, which proceed via an oxygen-bound sulfonamide intermediate ($\mathbf{5_{Ms}}$). As described in detail below, this

DOI: 10.1021/jacs.6b02714
J. Am. Chem. Soc. 2016, 138, 6049−6060

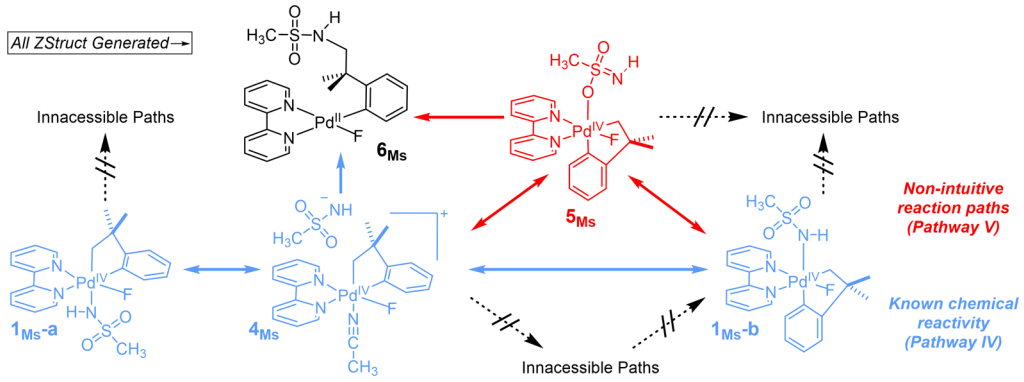

Figure 6. Overview of ZStruct search of the reactivity of $\mathbf{1_{Ms}}$-**a** involving multiple unproductive search paths as well as known and unknown chemical reactivity. Shown in blue are expected chemical reactivity, while red highlights the nonintuitive reaction paths.

unanticipated pathway is critical to explain the observed trends in rate as a function of sulfonamide substitution. A complete discussion of the computational results is provided below.

3.4. ZStruct Pathways for Isomerization. ZStruct generated two low barrier mechanisms for the isomerization of $\mathbf{1_{Ms}}$-**a** to $\mathbf{1_{Ms}}$-**b** (Figure 7). In the first elementary step, $\mathbf{TS7_{Ms}}$, the Pd–

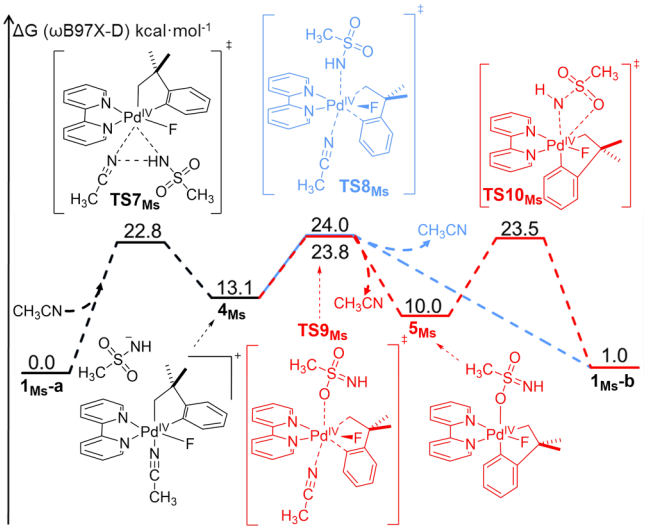

Figure 7. Two pathways for isomerization of $\mathbf{1_{Ms}}$-**a** to $\mathbf{1_{Ms}}$-**b**.

$NHSO_2CH_3$ bond of $\mathbf{1_{Ms}}$-**a** is exchanged for a Pd–$NCCH_3$ bond to generate intermediate $\mathbf{4_{Ms}}$.[40] Complex $\mathbf{4_{Ms}}$ then undergoes sulfonamide binding and concomitant reorganization of the aryl backbone to afford isomer $\mathbf{1_{Ms}}$-**b** through $\mathbf{TS8_{MS}}$. The computed ΔG^0 was 1.0 kcal·mol^{-1}, which agrees with the experimentally measured 0.94 ± 0.05 kcal·mol^{-1} at 65 °C.

The second isomerization pathway proceeds via displacement of $MsNH^-$ by CH_3CN to form $\mathbf{4_{Ms}}$, but then follows a unique path compared to the first isomerization mechanism. From $\mathbf{4_{Ms}}$, coordination of the sulfonamide through one of its oxygen atoms leads to $\mathbf{5_{Ms}}$ via $\mathbf{TS9_{Ms}}$. This O-bound sulfonamide intermediate then undergoes a concerted exchange of the sulfonamide oxygen with nitrogen at the palladium center via $\mathbf{TS10_{Ms}}$ to form the product $\mathbf{1_{Ms}}$-**b**. Notably, the κ^2-coordination seen in $\mathbf{TS10_{Ms}}$ resembles that of bidentate sulfonamide-ligated Pd^{IV} intermediates proposed by Ritter and co-workers.[14] The similarity in the activation barriers for the two mechanisms in Figure 7 ($\Delta\Delta G^{\ddagger}$ = 0.2 kcal·mol^{-1}) suggests that they likely occur competitively.

The experimental value of $\Delta G^{\ddagger}$ for isomerization (24.4 kcal·mol^{-1} at 65 °C) is in close agreement with the computed barriers of 24.0 and 23.8 kcal·mol^{-1} for the mechanisms in Figure 7. The computation is also consistent with the experimental observation that the isomerization process is zero order in sulfonamide. Furthermore, the ordered conformation of the sulfonamide approach as well as the presence of a stabilizing CH_3CN ligand in $\mathbf{TS8_{Ms}}$ and $\mathbf{TS9_{Ms}}$ are both consistent with the experimentally measured $\Delta S^{\ddagger}$ value of −14.8 ± 3.4 cal·K^{-1}·mol^{-1}.

While searching for reaction pathways connecting the observable isomers ($\mathbf{1_{Ms}}$-**a** to $\mathbf{1_{Ms}}$-**b**), three additional pathways were found leading to experimentally unobserved isomers (Figure 8). All three of these isomers ($\mathbf{1_{Ms}}$-**c**, $\mathbf{1_{Ms}}$-**d**, and $\mathbf{1_{Ms}}$-**e**)

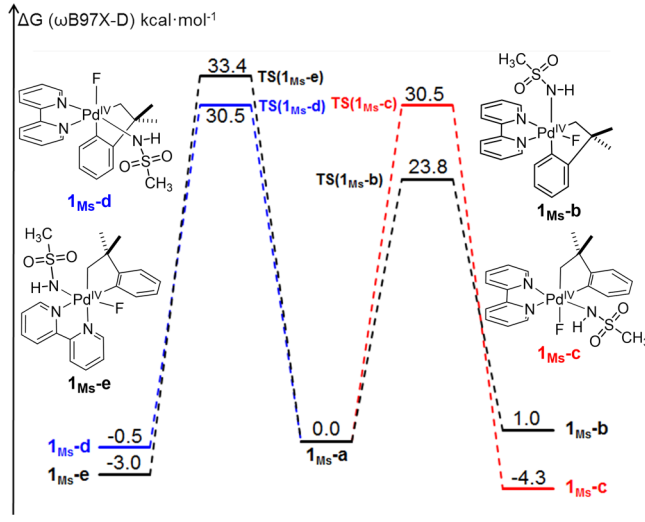

Figure 8. Energy barriers for pathways leading to the formation of $\mathbf{1_{Ms}}$ isomers (see Supporting Information for full reaction pathways).

were calculated to be more thermodynamically stable than $\mathbf{1_{Ms}}$-**a** and $\mathbf{1_{Ms}}$-**b**. However, the only kinetically viable pathway for isomerization connects $\mathbf{1_{Ms}}$-**a** and $\mathbf{1_{Ms}}$-**b**.[41] Overall, these results are consistent with the observation that $\mathbf{1_{Ms}}$-**a** and $\mathbf{1_{Ms}}$-**b** are the only isomers detected experimentally (Scheme 1 and Figure 4), and indicate that the other isomers are not kinetically relevant intermediates.

DOI: 10.1021/jacs.6b02714
J. Am. Chem. Soc. 2016, 138, 6049–6060

3.5. ZStruct Evaluation of C(sp^3)−N Bond-Forming Reductive Elimination. After ruling out the participation of other Pd^{IV} isomers, we analyzed possible pathways leading from $\mathbf{1_{Ms}}$**-a** and $\mathbf{1_{Ms}}$**-b** to C(sp^3)−N bond-forming reductive elimination.[42,43] ZStruct identified the proposed pathways **II**−**IV** as well as an unanticipated pathway, **V**. ZStruct predicts that pathway **II** is energetically inaccessible ($\Delta G^{\ddagger}$ > 32.0 kcal/mol; see Supporting Information for complete details). This is consistent with the experimental results, which provided evidence against this mechanism. In addition, the direct reductive elimination pathway (**III**) did not pass the screening criteria of Figure 5, as it has a calculated $\Delta G^{\ddagger}$ of 51.7 kcal·mol^{-1} (see Supporting Information for details). As such, the discussion below focuses on pathway **IV** as well as the new mechanism identified by ZStruct (pathway **V**).

3.5.1. Pathway IV. ZStruct found that the lowest energy route for C(sp^3)−N coupling starting from $\mathbf{1_{Ms}}$**-a** is a two-step sequence (pathway **IV** in Scheme 6). The first step involves the pre-equilibrium exchange of MsNH$^-$ for CH_3CN ($\mathbf{TS7_{Ms}}$) to generate an octahedral Pd^{IV} acetonitrile complex, $\mathbf{4_{Ms}}$ (Figure 9). Rate- limiting C(sp^3)−N bond-formation then proceeds via outer sphere S_N2-type attack of MsNH$^-$ on the axial sp^3-carbon ligand ($\mathbf{TS11_{Ms}}$, Figure 10).

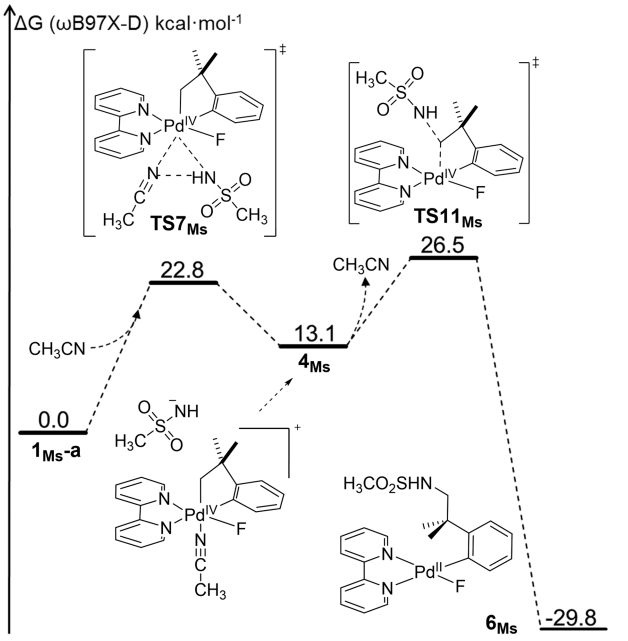

Figure 9. Pathway **IV**. C(sp^3)−N reductive elimination pathway from $\mathbf{1_{Ms}}$**-a**.

The nucleophile has an approach angle of 143.3° (compared to the ideal 180° in a traditional S_N2 reaction), highlighting the steric constraints of this transition state. The calculated value of $\Delta G^{\ddagger}$ (26.5 kcal·mol^{-1} at 65 °C) matches well with that observed experimentally (25.7 kcal·mol^{-1}). Importantly, related S_N2-like mechanisms for C(sp^3)−heteroatom reductive elimination have been proposed at platinum,[3] palladium,[44] and rhodium.[45] However, the S_N2-nature of $\mathbf{TS11_{Ms}}$ is particularly noteworthy considering that the participating carbon is a highly hindered neopentyl-type center.[12]

3.5.2. Pathway V. A second low energy pathway for C−N bond formation was identified by ZStruct and originates from $\mathbf{1_{Ms}}$**-b**. Interestingly, this mechanism (pathway **V**) is not among those initially hypothesized above, and has much less precedent in the literature.[13] As shown in Scheme 10, pathway **V** involves

Scheme 10. Pathway V from $\mathbf{1_{Ms}}$-b

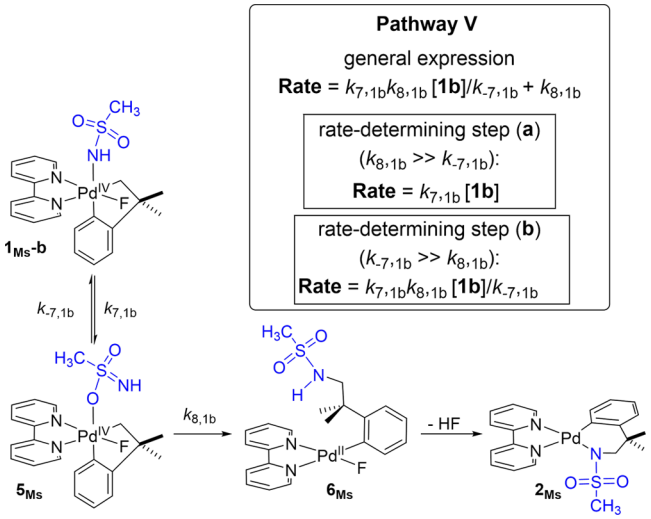

a two-step sequence, in which an initial nitrogen−oxygen exchange of the sulfonamide at the Pd center is followed by reductive elimination via an inner sphere concerted 5-membered transition state. Since the second step is calculated to be rate determining, the rate expression for this pathway is fully consistent with the experimental kinetic orders. The complete reaction profile for C(sp^3)−N bond formation from $\mathbf{1_{Ms}}$**-b** is shown in Figure 11. The calculated value of $\Delta G^{\ddagger}$ for the highest energy transition state of pathway **IV** (26.7 kcal·mol^{-1} at 65 °C) is very similar to that for pathway **V** (26.5 kcal·mol^{-1} at 65 °C). This suggests that the two pathways occur at comparable rates in this system.

As shown in Figure 11, the inner sphere C(sp^3)−N coupling in pathway **V** proceeds via backside attack, analogous to the

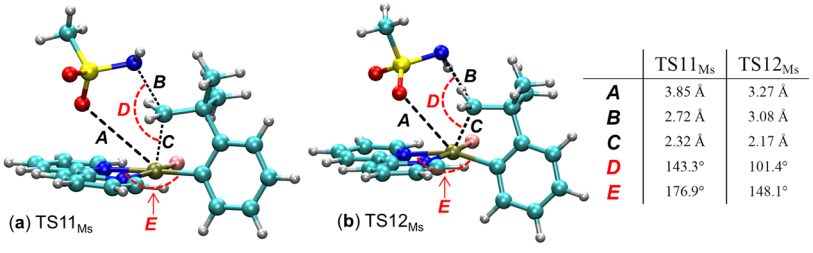

	$TS11_{Ms}$	$TS12_{Ms}$
A	3.85 Å	3.27 Å
B	2.72 Å	3.08 Å
C	2.32 Å	2.17 Å
D	143.3°	101.4°
E	176.9°	148.1°

Figure 10. (a) C(sp^3)−N reductive elimination transition state $\mathbf{TS11_{Ms}}$ from $\mathbf{1_{Ms}}$**-a** (in Pathway **IV**). (b) C(sp^3)−N reductive elimination transition state $\mathbf{TS12_{Ms}}$ from $\mathbf{1_{Ms}}$**-b** (in Pathway **V**).

DOI: 10.1021/jacs.6b02714
J. Am. Chem. Soc. 2016, 138, 6049−6060

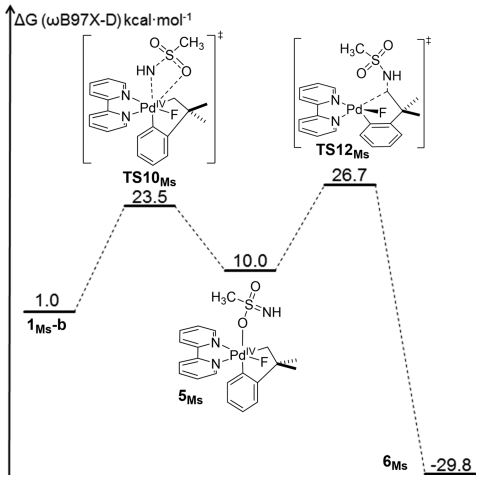

Figure 11. Pathway **V**. C(sp^3)–N reductive elimination from $\mathbf{1_{Ms}}$-**b**. All energies are referenced to $\mathbf{1_{Ms}}$-**a**.

outer-sphere S_N2-type mechanism of pathway **IV**. As such, stereochemical labeling studies would not be effective for experimentally distinguishing between pathways **IV** and **V**. However, the bond angle for approach of the sulfonamide in $\mathbf{TS12_{Ms}}$ is much shallower than that in pathway **V** (101.4° in comparison to 143.3°). This is due to a sustained stabilizing Pd–O interaction in the transition state, where the Pd–O distance is 3.27 Å for $\mathbf{TS12_{Ms}}$, compared to 3.85 Å in $\mathbf{TS11_{Ms}}$ (Figure 10). Other key bond lengths and angle comparisons are given in Figure 10, and these values are summarized for all of sulfonamides in the Supporting Information.

Because they are both S_N2 reactions with similar rate expressions, $\mathbf{TS11_{Ms}}$ and $\mathbf{TS12_{Ms}}$ might be initially considered chemically indistinguishable. However, in practice, there are a number of key differences including transition state structure (quantitatively different angles and bond lengths, Figure 10), inner vs outer sphere mechanism, and activation barriers. As will be shown below, the differences in reaction mechanism lead to changes in mechanism (pathway **IV** vs **V**) as a function of sulfonamide structure.

3.6. Computational Sulfonamide Screen and Experimental Verification. To further assess the feasibility of the proposed pathways, we computationally analyzed reductive elimination through pathways **IV** and **V** for the sulfonamides $TfNH^-$, $CF_2HSO_2NH^-$, $TsNH^-$, and $TsMeN^-$. As summarized in Table 4 and Figure 12, the lowest calculated barriers and experimental $\Delta G^{\ddagger}$ values for the five sulfonamides are in excellent agreement (R^2 = 0.90).

The predicted lowest energy pathway (i.e., **IV** versus **V**) was found to vary as a function of sulfonamide structure. For the sulfonamides $CF_2HSO_2NH^-$ and $CH_3SO_2NH^-$, pathways **IV** and **V** have similar values of $\Delta G^{\ddagger}$, while $TsNH^-$ favors pathway **IV**. In contrast, $TsMeN^-$ and $TfNH^-$ favor pathway **V**. For all five sulfonamides, the calculated $\Delta G^{\ddagger}$ for pathway **IV** generally correlates with pK_a, with higher pK_a's affording higher barriers. (A linear regression of $\Delta G^{\ddagger}$ for pathway **IV** versus pK_a has an R^2 = 0.77).

This trend is consistent with results from Goldberg's group studying C(sp^3)–O coupling at Pt^{IV}. Specifically, they showed a linear Hammett plot (ρ = +1.44) upon varying the substituents on the benzoate nucleophile.[19e] A key consequence of this pK_a trend is that the most basic sulfonamide ($TsMeN^-$) has a prohibitively high barrier for reductive elimination via pathway

Table 4. Comparison of Lowest Barrier Calculated C(sp^3)–N Reductive Elimination and Experimentally Measured $\Delta G^{\ddagger}$ Values for Various Sulfonamides

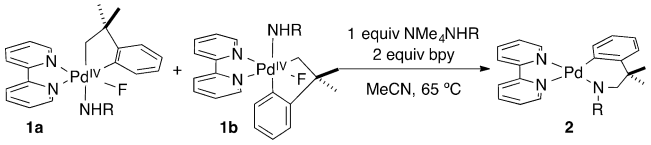

R	pK_a[a]	Path. IV[b] $\Delta G^{\ddagger}_{DFT}$	Path. V[c] $\Delta G^{\ddagger}_{DFT}$	$\Delta G^{\ddagger}_{Exp}$
CF_3SO_2 (Tf)	6.37	25.3	24.4	24.8
CF_2HSO_2	7.46	24.7	25.1	25.1
p-Tol-SO_2NH (Ts)	10.26	26.1	28.5	25.7
CH_3SO_2 (Ms)	10.87	26.5	26.7	25.7
p-Tol-SO_2NCH_3 (TsNMe)	11.67	27.8	25.2	25.0

[a] pK_a values from the literature database of ACD/Laboratories Software version 11.02. [b] From $\mathbf{1_{Ms}}$-**a**. [c] From $\mathbf{1_{Ms}}$-**b**.

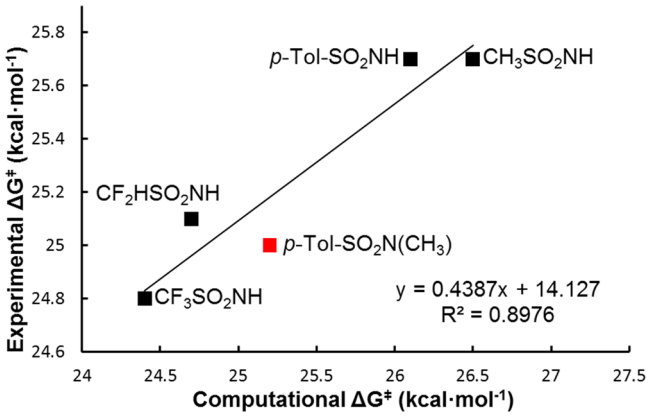

Figure 12. Comparison between computational and experimental $\Delta G^{\ddagger}$ for C(sp^3)–N reductive elimination. The point computation predicted prior to experiment is highlighted in red.

IV. As such, the relatively fast rate of reductive elimination with this nucleophile is due to the accessibility of pathway **V**, which does not trend with pK_a (a linear regression for the five sulfonamides has R^2 = 0.28).

The factors controlling the relative barriers for pathway **V** as a function of sulfonamide appear to be complex, and we have not been able to identify clear trends in $\Delta G^{\ddagger}$ as a function of pK_a or bond lengths/bond angles that fit for all of the sulfonamides. Nonetheless, one instructive comparison for pathway **V** is between $TsHN^-$ and $TsMeN^-$, which differ only by substitution of a hydrogen for a methyl group on the sulfonamide. As shown in Table 4, this change results in a 3.3 kcal·mol^{-1} decrease in $\Delta G^{\ddagger}$ for pathway **V**, thereby enabling fast reductive elimination from the $TsMeN^-$ complex via this pathway. A carefully comparison of these systems shows that, with $TsNH^-$, the transition state for C–N bond formation via pathway **V** requires breaking a Ts–N–H···F–Pd hydrogen bond. This hydrogen-bond breaking is clearly reflected in the increasing H···F distance moving from $\mathbf{5_{Ts}}$ (2.01 Å) to transition state $\mathbf{TS12_{Ts}}$ (3.05 Å) to the product $\mathbf{6_{Ts}}$ (4.80 Å). Importantly, a similar hydrogen bond is not possible in the analogous intermediate $\mathbf{5_{TsNMe}}$, since the hydrogen bond donor has been replaced with a methyl group. The magnitude of $\Delta\Delta G^{\ddagger}$ between the two sulfonamides for pathway **V** (3.3 kcal/mol) is fully consistent with the penalty associated with

DOI: 10.1021/jacs.6b02714
J. Am. Chem. Soc. 2016, 138, 6049–6060

breaking a hydrogen bond. As such, we propose that the lack of a H-bond donor in $TsMeN^-$ is likely responsible for the preferred mechanism for C(sp^3)–N reductive elimination, and enables fast C–N bond-formation despite the high pK_a of this sulfonamide.

Overall, the computational activation barriers for the five sulfonamides agree well with experiment (Figure 12), but only when taking into account two distinct mechanistic routes, pathways **IV** and **V**. Furthermore, while pathway **IV** is computed to be the lowest (or approximately equal) barrier mechanism for 3 of the 5 sulfonamides, $\mathbf{1}_{\mathbf{TsNMe}}$ has a much lower barrier for pathway **V**. Pathway **V** is also favored for $\mathbf{1}_{\mathbf{Tf}}$, but in this case, the energy difference between pathways **IV** and **V** is less significant ($\Delta\Delta G^{\ddagger}$ < 1 kcal·mol^{-1}). These observations are consistent with the experimental activation entropies. The $\Delta S^{\ddagger}$ values for C(sp^3)–N coupling from $\mathbf{1}_{\mathbf{Tf}}$ and $\mathbf{1}_{\mathbf{TsNMe}}$ are similar (−4.9 and −3.4 cal·K^{-1}·mol^{-1}) and clearly distinct from $\Delta S^{\ddagger}$ for $\mathbf{1}_{\mathbf{Ms}}$ (−23.5 cal·K^{-1}·mol^{-1}). The higher $\Delta S^{\ddagger}$ likely reflects the increased order associated with solvation of the charged intermediates/transition state in pathway **IV** versus the neutral compounds in pathway **V**. This demonstrates that both predicted mechanisms are critical for understanding the observed rates.

3.7. Additional Predictions Based on Thermodynamic Considerations. We next sought to computationally examine the impact of moving to the sulfonamide Tf_2N^-, which has an even lower pK_a than that of $TfNH^-$. The studies described above suggest that the Pd^{IV} complex of this sulfonamide ($\mathbf{1}_{\mathbf{BisTf}}$) should react at a fast rate via pathway **IV**. Consistent with this hypothesis, the $\Delta G^{\ddagger}$ for C(sp^3)–N coupling from $\mathbf{1}_{\mathbf{BisTf}}$ via pathway **IV** is calculated to be 23.7 kcal·mol^{-1}. A significantly higher value (26.9 kcal·mol^{-1}) is calculated for pathway **V**. However, the simulations also predict that the C(sp^3)–N coupling product $\mathbf{6}_{\mathbf{BisTf}}$ is 5.5 kcal·mol^{-1} *uphill* from the starting material, $\mathbf{1}_{\mathbf{BisTf}}$. Therefore, C($sp^3$)–N coupling from $\mathbf{1}_{\mathbf{BisTf}}$ is predicted to be kinetically fast, but thermodynamically unfavorable (Figure 13).

The ZStruct assessment of $\mathbf{1}_{\mathbf{BisTf}}$ suggested that alternative, more thermodynamically favorable reductive elimination pathways are likely to occur with this complex. As such, we also computationally evaluated the pathway for C(sp^3)–C(sp^2) bond-forming reductive elimination from $\mathbf{1}_{\mathbf{BisTf}}$. This process is predicted to be thermodynamically downhill (−4.4 kcal·mol^{-1} to generate the initial intermediate $\mathbf{14}_{\mathbf{BisTf}}$), with a computed activation barrier of 23.3 kcal·mol^{-1} (Figure 13). To test these computational predictions, we conducted the thermolysis of a mixture of **3** with 2 equiv of NMe_4NTf_2 in CD_3CN at 65 °C. As anticipated, none of the thermodynamically disfavored product of C(sp^3)–N bond-forming reductive elimination ($\mathbf{6}_{\mathbf{BisTf}}$) was detected. Instead, the C(sp^2)–C(sp^3) bond-forming reductive elimination product, cyclobutane **15**, was obtained in quantitative yield (Scheme 11). The activation barrier for the formation of **15** was measured experimentally as 23.8 kcal·mol^{-1}. This is in excellent agreement with the computational prediction of 23.3 kcal·mol^{-1}.

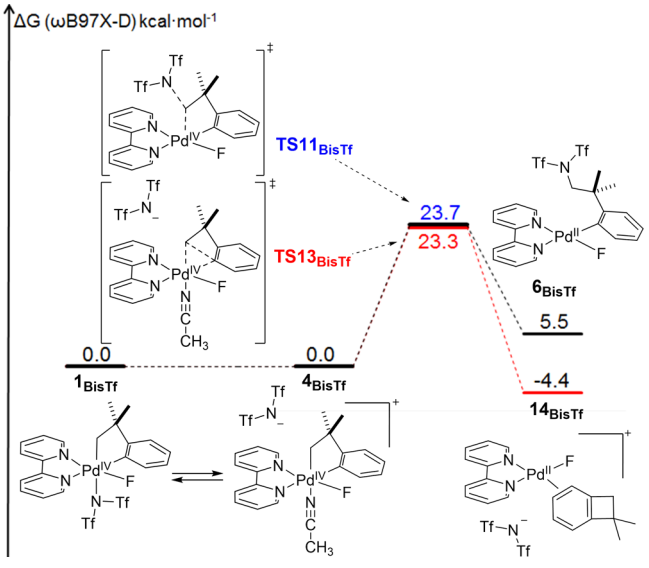

Figure 13. C(sp^3)–N versus C(sp^3)-C(sp^2) reductive elimination from common pentacoordinate intermediate $\mathbf{4}_{\mathbf{BisTf}}$. All energies referenced to $\mathbf{1}_{\mathbf{BisTf}}$-**a**.

Scheme 11. Thermolysis of 3 in the Presence of NMe_4NTf_2

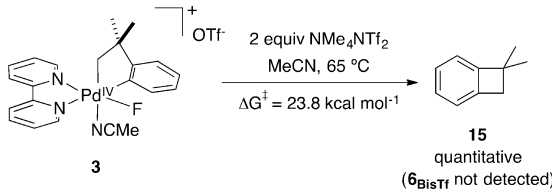

CONCLUSIONS

Detailed mechanistic investigations of reductive elimination from octahedral Pd^{IV} complexes are challenging due to the presence of multiple isomers and the feasibility of multiple kinetically indistinguishable pathways. In this report, we disclose a combined experimental and simulation investigation of competing isomerization and C(sp^3)–N bond-forming reductive elimination from a series of Pd^{IV} complexes. Several possible pathways could be ruled out through experimental investigations, but numerous plausible mechanisms proved to be experimentally indistinguishable.

These challenges were addressed by using ZStruct, a computational reaction discovery method, to explore this complicated chemical landscape. ZStruct enabled us to rapidly rule out pathways involving unobservable isomers and to establish an isomerization mechanism within 1 kcal·mol^{-1} of the experimentally determined $\Delta G^{\ddagger}$.

In addition, two low energy mechanisms for C(sp^3)–N bond-formation were identified: an S_N2-type outer sphere C–N coupling (pathway **IV**) and a concerted inner sphere C–N bond formation that proceeds via a 5-membered transition state from an O-bound sulfonamide intermediate (pathway **V**). Pathway **V** appears to be the major pathway for reductive elimination for some sulfonamides. This hitherto unreported pathway therefore merits consideration in any future studies of C(sp^3)–N reductive elimination reactions of sulfonamide derivatives.

Taking into account competition between these two mechanisms, ZStruct results showed good agreement with the experimentally measured values of $\Delta G^{\ddagger}$ for C(sp^3)–N bond-forming reductive elimination with stereoelectronically varied sulfonamides. Across a variety of substrates, competition between pathways **IV** and **V** needs to be accounted for to accurately predict and explain experimental outcomes. In one case, computation also predicted that C(sp^2)–C(sp^3) reductive

DOI: 10.1021/jacs.6b02714
J. Am. Chem. Soc. 2016, 138, 6049–6060

elimination would occur instead of the kinetically facile, yet thermodynamically disfavored C(sp^3)–N coupling from $\mathbf{1}_{BisTf}$.

This study contributes to a growing body of work demonstrating the advantages of a combined simulation and experimental approach to mechanistic investigations, especially those pertaining to organometallic complexes.[46] Moving forward, we plan to use this approach to evaluate the full suite of possible reductive elimination reactions from $\mathbf{1}_{Ms}$ and its analogues (i.e., competing C(sp^3)–N, C(sp^2)–N, C(sp^3)–F, C(sp^2)–F, and C(sp^3)–C(sp^2) reductive elimination). Overall, this work demonstrates that the combination of experimental mechanistic studies with ZStruct holds great promise for the detailed evaluation of complex reaction mechanisms.

■ ASSOCIATED CONTENT

Supporting Information

The Supporting Information is available free of charge on the ACS Publications website at DOI: 10.1021/jacs.6b02714.

Experimental procedures and complete characterization for all new compounds (PDF)

Computational methods, alternative pathways generated by ZStruct, XYZ coordinates and energies for all structures (PDF)

Crystallographic data for compounds $\mathbf{1}_{TsNMe}$-**b**, $\mathbf{2}_{Ms}$, $\mathbf{2}_{Tf}$, and $\mathbf{2}_{TsNMe}$ (CIF)

■ AUTHOR INFORMATION

Corresponding Authors

*paulzim@umich.edu

*mssanfor@umich.edu

Author Contributions

‡I.M.P. and M.H.P.-T. contributed equally.

Notes

The authors declare no competing financial interest.

■ ACKNOWLEDGMENTS

This work was supported by the National Science Foundation Grants CHE-1361542 and CHE-1551994. We acknowledge Dr. Jeff Kampf for X-ray crystallographic analysis of $\mathbf{1}_{TsNMe}$-**b**, $\mathbf{2}_{Ms}$, $\mathbf{2}_{Tf}$, and $\mathbf{2}_{TsNMe}$ as well as funding from NSF Grant CHE-0840456 for X-ray instrumentation. I.M.P. acknowledges the NSF for a graduate research fellowship (CHE-1256260). M.H.P.-T. acknowledges support from a Foundation Ramón Areces Fellowship. The authors thank Dr. Amanda Cook-Sneathen and Dr. Christo Sevov for helpful discussions. The authors also thank David Braun for support in computational administration.

■ REFERENCES

(1) For some examples of Pd^{II}-catalyzed C(sp^3)-H amination see: (a) McNally, A.; Haffemayer, B.; Collins, B. S. L.; Gaunt, M. J. *Nature* **2014**, *510*, 129. (b) Sun, W.-W.; Cao, P.; Mei, R.-Q.; Li, Y.; Ma, Y.-L.; Wu, B. *Org. Lett.* **2014**, *16*, 480. (c) Ye, X.; He, Z.; Ahmed, T.; Weise, K.; Akhmedov, N. G.; Petersen, J. L.; Shi, X. *Chem. Sci.* **2013**, *4*, 3712. (d) Zhang, Q.; Chen, K.; Rao, W.-H.; Zhang, Y.; Chen, F.-J.; Shi, B.-F. *Angew. Chem., Int. Ed.* **2013**, *52*, 13588. (e) Iglesias, Á.; Álvarez, R.; de Lera, Á. R.; Muñiz, K. *Angew. Chem., Int. Ed.* **2012**, *51*, 2225. (f) Nadres, E. T.; Daugulis, O. *J. Am. Chem. Soc.* **2012**, *134*, 7. (g) He, G.; Zhao, Y.; Zhang, S.; Lu, C.; Chen, G. *J. Am. Chem. Soc.* **2012**, *134*, 3.

(2) Amination of alkenes see: (a) Martínez, C.; Wu, Y.; Weinstein, A. B.; Stahl, S.; Liu, G.; Muñiz, K. *J. Org. Chem.* **2013**, *78*, 6309. (b) Muñiz, K.; Martínez, C. *J. Org. Chem.* **2013**, *78*, 2168. (c) Xiong, T.; Li, Y.; Mao, L.; Zhang, Q.; Zhang, Q. *Chem. Commun.* **2012**, *48*, 2246. (d) Xu, T.; Qiu, S.; Liu, G. *J. Organomet. Chem.* **2011**, *696*, 46. (e) Liskin, D. V.; Sibbald, P. A.; Rosewall, C. F.; Michael, F. E. *J. Org. Chem.* **2010**, *75*, 6294. (f) Iglesias, Á.; Pérez, E. G.; Muñiz, K. *Angew. Chem., Int. Ed.* **2010**, *49*, 8109. (g) Sibbald, P. A.; Michael, F. E. *Org. Lett.* **2009**, *11*, 1147. (h) Rosewall, C. F.; Sibbald, P. A.; Liskin, D. V.; Michael, F. E. *J. Am. Chem. Soc.* **2009**, *131*, 9488. (i) Sibbald, P. A.; Rosewall, C. F.; Swartz, R. D.; Michael, F. E. *J. Am. Chem. Soc.* **2009**, *131*, 15945. (j) Muñiz, K.; Hövelmann, C. H.; Streuff, J. *J. Am. Chem. Soc.* **2008**, *130*, 763. (k) Muñiz, K. *J. Am. Chem. Soc.* **2007**, *129*, 14542. (l) Minatti, A.; Muñiz, K. *Chem. Soc. Rev.* **2007**, *36*, 1142. (m) Streuff, J.; Hövelmann, C. H.; Nieger, M.; Muñiz, K. *J. Am. Chem. Soc.* **2005**, *127*, 14586.

(3) For mechanistic study on C(sp^3)–N bond-forming reductive elimination from Pt^{IV}, see: Pawlikowski, A. V.; Getty, A. D.; Goldberg, K. I. *J. Am. Chem. Soc.* **2007**, *129*, 10382.

(4) Iglesias, Á.; Muñiz, K. *Helv. Chim. Acta* **2012**, *95*, 2007.

(5) Pérez-Temprano, M. H.; Racowski, J. M.; Kampf, J. W.; Sanford, M. S. *J. Am. Chem. Soc.* **2014**, *136*, 4097.

(6) The 2 equiv of bpy is added to limit 2° side reactions of the reductive elimination product (i.e., substitution of the bpy ligand of $\mathbf{2}_{Ts}$ with $TsNH^-$). It is not believed to impact the mechanism of the C(sp^3)–N coupling reaction. See ref 5 for additional information.

(7) (a) Zimmerman, P. M. *J. Comput. Chem.* **2013**, *34*, 1385. (b) Zimmerman, P. M. *Mol. Simul.* **2015**, *41*, 43. (c) Zimmerman, P. M. *J. Comput. Chem.* **2015**, *36*, 601. (d) Zimmerman, P. *J. Chem. Theory Comput.* **2013**, *9*, 3043. (e) Zimmerman, P. M. *J. Chem. Phys.* **2013**, *138*, 184102.

(8) The cost of the search was approximately 80 000 computing hours, which corresponds to less than 1 week of computational time on 1000 CPUs.

(9) For other recent publications demonstrating chemical exploration software see: (a) Wang, L.-P.; Titov, A.; McGibbon, R.; Liu, F.; Pande, V. S.; Martínez, T. J. *Nat. Chem.* **2014**, *6*, 1044–1048. (b) Rappoport, D.; Galvin, C. J.; Zubarev, D. Y.; Aspuru-Guzik, A. *J. Chem. Theory Comput.* **2014**, *10*, 897–907. (c) Maeda, S.; Morokuma, K. *J. Chem. Theory Comput.* **2011**, *7*, 2335–2345. (d) Maeda, S.; Taketsugu, T.; Morokuma, K. *J. Comput. Chem.* **2014**, *35*, 166–173. (e) Ohno, K.; Maeda, S. *Chem. Phys. Lett.* **2004**, *384*, 277–282. (f) Maeda, S.; Ohno, K.; Morokuma, K. *Phys. Chem. Chem. Phys.* **2013**, *15*, 3683–3701. (g) Bergeler, M.; Simm, G. N.; Proppe, J.; Reiher, M. *J. Chem. Theory Comput.* **2015**, *11*, 5712–5722.

(10) Byers, P. K.; Canty, A. J.; Crespo, M.; Puddephatt, R. J.; Scott, J. D. *Organometallics* **1988**, *7*, 1363–1367.

(11) Dick, A. R.; Kampf, J. W.; Sanford, M. S. *J. Am. Chem. Soc.* **2005**, *127*, 12790–12791.

(12) Camasso, N. M.; Pérez-Temprano, M. H.; Sanford, M. S. *J. Am. Chem. Soc.* **2014**, *136*, 12771.

(13) For a proposal of related pathways for C–O bond-forming reductive elimination with carboxylate nucleophiles, see: Gary, J. B.; Sanford, M. S. *Organometallics* **2011**, *30*, 6143.

(14) Furuya, T.; Benitez, D.; Tkatchouk, E.; Strom, A. E.; Tang, P.; Goddard, W. A.; Ritter, T. *J. Am. Chem. Soc.* **2010**, *132*, 3793–3807.

(15) Pawlikowski, A. V.; Getty, A. D.; Goldberg, K. I. *J. Am. Chem. Soc.* **2007**, *129*, 10382–10393.

(16) For recent reviews on Pd^{IV} reductive elimination please see: (a) Muñiz, K. *Angew. Chem., Int. Ed.* **2009**, *48*, 9412–9423. (b) Sehnal, P.; Taylor, R. J. K.; Fairlamb, I. J. S. *Chem. Rev.* **2010**, *110*, 824–889. (c) Xu, L.-M.; Li, B.-J.; Yang, Z.; Shi, Z.-J. *Chem. Soc. Rev.* **2010**, *39*, 712–733.

(17) For S_N2-mechanism of C(sp^3)-X (pathway I) from Pt^{IV} see: Shilov, A. E.; Shul'pin, G. B. *Chem. Rev.* **1997**, *97*, 2879.

(18) Literature precedents for pathway **II** see: (a) Arthur, K. L.; Wang, Q. L.; Bregel, D. M.; Smythe, N. A.; O'Neill, B. A.; Goldberg, K. I.; Moloy, K. G. *Organometallics* **2005**, *24*, 4624. (b) Crumpton-Bregel, D. M.; Goldberg, K. I. *J. Am. Chem. Soc.* **2003**, *125*, 9442. (c) Crumpton, D. M.; Goldberg, K. I. *J. Am. Chem. Soc.* **2000**, *122*, 962.

DOI: 10.1021/jacs.6b02714
J. Am. Chem. Soc. 2016, 138, 6049–6060

(19) Literature precedents for reductive elimination from cationic species (pathways **III** and **V**) see: (a) Smythe, N. A.; Grice, K. A.; Williams, B. S.; Goldberg, K. I. *Organometallics* **2009**, *28*, 277. (b) Khusnutdinova, J. R.; Newman, L. L.; Zavalij, P. Y.; Lam, Y.-F.; Vedernikov, A. N. *J. Am. Chem. Soc.* **2008**, *130*, 2174. (c) Khusnutdinova, J. R.; Zavalij, P. Y.; Vedernikov, A. N. *Organometallics* **2007**, *26*, 3466. (d) Vedernikov, A. N.; Binfield, S. A.; Zavalij, P. Y.; Khusnutdinova, J. R. *J. Am. Chem. Soc.* **2006**, *128*, 82. (e) Williams, B. S.; Goldberg, K. I. *J. Am. Chem. Soc.* **2001**, *123*, 2576. (f) Williams, B. S.; Holland, A. W.; Goldberg, K. I. *J. Am. Chem. Soc.* **1999**, *121*, 252.

(20) Literature precedents for pathway **IV** see: (a) Rivada-Wheelaghan, O.; Roselló-Merino, M.; Díez, J.; Maya, C.; López-Serrano, J.; Conejero, S. *Organometallics* **2014**, *33*, 5944. (b) Rivada-Wheelaghan, O.; Ortuño, M. A.; Díez, J.; García-Garrido, S. E.; Maya, C.; Lledós, A.; Conejero, S. *J. Am. Chem. Soc.* **2012**, *134*, 15261. (c) Crosby, S. H.; Thomas, H. R.; Clarkson, G. J.; Rourke, J. P. *Chem. Commun.* **2012**, *48*, 5775. (d) Zhao, S.-B.; Wang, R.-Y.; Nguyen, H.; Becker, J. J.; Gagné, M. R. *Chem. Commun.* **2012**, *48*, 443. (e) Khusnutdinova, J. R.; Newman, L. L.; Zavalij, P. Y.; Lam, Y.-F.; Vedernikov, A. N. *J. Am. Chem. Soc.* **2008**, *130*, 2174.

(21) The sulfonamide exchange cannot take place by an associative mechanism since $\mathbf{1}_{Ts}$ is coordinatively saturated.

(22) Rate studies were performed under our optimal conditions, using 1 equiv of bpy as an additive. As discussed in our previous communication (ref 5), the bpy is added to prevent decomposition of the reductive elimination product **2**, but does not impact the C−N coupling process (see ref 6).

(23) The observed first-order dependence of [Pd] rules out reductive elimination mechanisms involving two palladium centers.

(24) The observed zero-order dependence on sulfonamide rules out mechanisms that involve displacement of the fluoride ligand with an equivalent of exogeneous sulfonamide prior to reductive elimination.

(25) On the basis of this data, we can also rule out the formation of a Pd^{IV} intermediate with two N-ligands and subsequent C−N reductive elimination. This pathway would also be expected to show a first-order dependence on sulfonamide.

(26) For related experiments, see: (a) Racowski, J. M.; Dick, A. R.; Sanford, M. S. *J. Am. Chem. Soc.* **2009**, *131*, 10974. (b) Dick, A. R.; Kampf, J. W.; Sanford, M. S. *J. Am. Chem. Soc.* **2005**, *127*, 12790.

(27) The isomerization process was studied in the presence of excess of NMe_4NR to avoid reductive elimination processes during the measurement of the equilibrium. A zeroth-order dependence on [NMe_4NR] was observed for this step.

(28) Similar models were applied to TfNH and TsNMe.

(29) (a) Mendes, P. *Bioinformatics* **1993**, *9*, 563. (b) Mendes, P. *Trends Biochem. Sci.* **1997**, *22*, 361. (c) Mendes, P.; Kell, D. B. *Bioinformatics* **1998**, *14*, 869. (d) Martins, A. M.; Mendes, P.; Cordeiro, C.; Freire, A. P. *Eur. J. Biochem.* **2001**, *268*, 3930.

(30) (a) Sun, Z.; Winschel, G. A.; Zimmerman, P. M.; Nagorny, P. *Angew. Chem., Int. Ed.* **2014**, *53*, 11194−11198. (b) Ludwig, J. R.; Zimmerman, P. M.; Gianino, J. B.; Schindler, C. S. *Nature*, **2016**, in press. DOI: 10.1038/nature17432.

(31) (a) Becke, A. D. *Phys. Rev. A: At., Mol., Opt. Phys.* **1988**, *38*, 3098−3100. (b) Becke, A. D. *J. Chem. Phys.* **1993**, *98*, 5648. (c) Lee, C.; Yang, W.; Parr, R. G. *Phys. Rev. B: Condens. Matter Mater. Phys.* **1988**, *37*, 785−789.

(32) (a) Hay, P. J.; Wadt, W. R. *J. Chem. Phys.* **1985**, *82*, 299. (b) Hay, P. J.; Wadt, W. R. *J. Chem. Phys.* **1985**, *82*, 270. (c) Hay, P. J.; Wadt, W. R. *J. Chem. Phys.* **1985**, *82*, 270. (d) Wadt, W. R.; Hay, P. J. *J. Chem. Phys.* **1985**, *82*, 284. (e) Dunning, T. H.; Hay, P. J. *Methods of Electronic Structure Theory, Vol. 2*; Schaefer, H. F., Ed.; Plenum Publishing Company Limited: New York, 1977.

(33) The smaller basis set was chosen as a compromise between cost and accuracy in expectation of the large sample size of initial screening process.

(34) While the initial calculations were not performed using solvent, the maximum solvent stabilization observed from gas phase to fully solvated was 10 kcal·mol^{-1}. Paths with $\Delta G^{\ddagger}$ above 40 kcal·mol^{-1} would still not compete with the rates observed for C(sp^3)−N R.E. or isomerization.

(35) For general paper on SMD: Marenich, A. V.; Cramer, C. J.; Truhlar, D. G. *J. Phys. Chem. B* **2009**, *113*, 6378−6396.

(36) Tomasi, J.; Mennucci, B.; Cammi, R. *Chem. Rev.* **2005**, *105*, 2999. (b) Cammi, R.; Tomasi, J. *J. Comput. Chem.* **1995**, *16*, 1449.

(37) Chai, J. D.; Head-Gordon, M. *Phys. Chem. Chem. Phys.* **2008**, *10*, 6615.

(38) Minenkov, Y.; Singstad, Å.; Occhipinti, G.; Jensen, V. R. *Dalton Trans.* **2012**, *41*, 5526.

(39) Calculations including CH_3CN were referenced to $\mathbf{1}_{Ms}$-**a**_withCH_3CN, calculations without CH_3CN are referenced to $\mathbf{1}_{Ms}$-**a**. For these structures see CIF file in the Supporting Information.

(40) In one system, the incorporation of an explicit solvent molecule of acetonitrile was crucial for accurate representation the isomerization shown in Figure 6. The barriers for sulfonamide dissociation (**TS6**) and isomerization (**TS9**) (**7** → **10**) were 2.9 and 3.4 kcal·mol^{-1} higher, respectively, without explicit solvent. This effect can be rationalized by the stabilizing interaction of acetonitrile's lone pair with the cationic palladium center.

(41) Pathways leading to $\mathbf{1}_{Ms}$-**c**, $\mathbf{1}_{Ms}$-**d**, $\mathbf{1}_{Ms}$-**e** from $\mathbf{1}_{Ms}$-**b** were found to be higher in energy than those originating from $\mathbf{1}_{Ms}$-**a**. These results are detailed in the Supporting Information.

(42) Since the reaction is zero order in sulfonamide and bpy does not have any effect in the C(sp^3)-N reductive elimination, we performed the calculations without the presence of exogeneous sulfonamide and bpy. Thus, we avoid the generation of intermediates and TS involving unproductive pathways and the analysis of those data that would require even more computer power and time.

(43) A single explicit solvent molecule or several (including sampling of the many possible solvent molecule arrangements) were attempted for each conformation. The lowest energy structures are reported.

(44) (a) Marquard, S. L.; Hartwig, J. F. *Angew. Chem., Int. Ed.* **2011**, *50*, 7119. (b) Marquard, S. L.; Rosenfeld, D. C.; Hartwig, J. F. *Angew. Chem., Int. Ed.* **2010**, *49*, 793.

(45) Sanford, M. S.; Groves, J. T. *Angew. Chem., Int. Ed.* **2004**, *43*, 588.

(46) For recent reviews detailing a combined computational and experimental approach to organometallic mechanisms, see: (a) Bonney, K. J.; Schoenebeck, F. *Chem. Soc. Rev.* **2014**, *43*, 6609. (b) Cheng, G.; Zhang, X.; Chung, L. W.; Xu, L.; Wu, Y. *J. Am. Chem. Soc.* **2015**, *137*, 1706−1725. (c) Jover, J.; Fey, N. *Chem. - Asian J.* **2014**, *9*, 1714. (d) Sperger, T.; Sanhueza, I. a.; Kalvet, I.; Schoenebeck, F. *Chem. Rev.* **2015**, *115*, 9532−9586.

DOI: 10.1021/jacs.6b02714
J. Am. Chem. Soc. 2016, 138, 6049−6060